ARTICLE NO. 80-0002R

Investigation of a Three-Dimensional Shock Wave Separated Turbulent Boundary Layer

M. I. Kussoy,* J. R. Viegas,* and C. C. Horstman†
NASA Ames Research Center, Moffett Field, Calif.

A detailed investigation of a flow in which a three-dimensional shock wave separates a two-dimensional turbulent boundary layer is presented. The resulting flowfield is highly three dimensional with a significant portion of flow separation on the surface at the $\phi = 0$ deg (windward) plane was well as a large zone of secondary surface flow off this plane. Mean and fluctuating experimental measurements were obtained throughout the entire flowfield. These measurements included mean pressures, flow angles and shear on the surface, as well as yaw angles, static pressures, turbulent shear stresses, and turbulent kinetic energies on selected planes throughout the flowfield. In addition, numerical predictions of this flow, obtained by solving the Navier-Stokes equations with an algebraic eddy viscosity turbulence model, are presented. These computations reasonably predict both the surface and flowfield quantities, despite the extremely complicated nature of the experimental flow.

Nomenclature

C_f = skin-friction coefficient, $2\tau_w/\rho_\infty u_\infty^2$
k = turbulent kinetic energy
p = static pressure
Re/m = Reynolds number per meter
T = static temperature
u,v,w = mass-averaged velocity components in x,y, and ϕ directions, respectively
x = axial coordinate parallel to test section centerline, measured from cone tip
y = radial coordinate, distance normal to wall
α = yaw angle, $\tan^{-1}(w/u)$
α_s = surface skin friction line angle, $\tan^{-1}[(\partial w/\partial y)_{y=0}/(\partial u/\partial y)_{y=0}]$
ρ = density
ϕ = azimuthal coordinate, measured from windward ray of cone

Subscripts

e = boundary-layer edge
t = turbulent
T = total
w = wall
x = axial component
∞ = freestream condition upstream of interaction

Introduction

HISTORICALLY, the scientific community has shown intense interest in the computation of realistic fluid dynamic situations such as the flow over control surfaces, wing-body interactions, and other protuberances on aircraft and missiles. With the advent of sophisticated computers equipped with huge memories and the parallel development of advanced computer codes, the computation of such complicated flows is rapidly approaching the practical state. One limiting aspect of computer codes is the choice of a turbulence model. A critical part of the development of any turbulence model is its testing against a wide range of experimental observations. Only after such comparisons are made can a computer code and its associated turbulence model be assessed. A major effort at NASA Ames Research Center has been concerned with devising "building block" experiments aimed at providing data of sufficient detail and accuracy to be used in an evaluation of computer code development.[1] In these experiments, which run the gamut from simple two-dimensional, flat-plate boundary-layer flows to the separated flow over three-dimensional supercritical wings, both mean and fluctuating flowfield quantities have been measured. Complete documentation of the flow is believed necessary for any meaningful evaluation of a turbulence model.

In a recent paper,[2] it was shown that a computer code employing a relatively simple algebraic turbulence model did an excellent job of predicting both the surface and mean flowfield quantities of a complex three-dimensional separated boundary-layer flow generated by a swept shock wave. However, the separated flow regions did not include any reversed flow in the two-dimensional sense. For the present study an experimental test flow was devised for separated three-dimensional boundary layers that includes a significant region of streamwise recirculation. This should provide a more severe test of the turbulence models employed in the computer codes.

The present flow is a fairly complicated one in which a three-dimensional shock wave impinges on and separates a two-dimensional supersonic turbulent boundary layer. In this paper, both mean and fluctuating data obtained on the surface and in the flowfield are presented. Numerical predictions obtained by solving the Navier-Stokes equations with an algebraic eddy viscosity turbulence model are presented and conclusions drawn concerning the relative abilities of this turbulence model to determine this type of flow a priori.

Description of Experiment

Facility

The experiment was conducted in Ames Research Center's high Reynolds number channel. This air-charged blowdown facility consists of a large settling tank with flow conditioning screens and interchangeable test sections and nozzles, each designed to produce a particular flow. For the present study a supersonic nozzle and a constant-diameter tube (diameter 24.17 cm, length 270 cm) were used. The nominal freestream test conditions were: total temperature = 278 K; total pressure = 1.0-9.0 atm; freestream unit Reynolds num-

Received Jan. 2, 1980; presented as Paper 80-0002 at the AIAA 18th Aerospace Sciences Meeting, Pasadena, Calif., Jan. 14-16, 1980; revision received July 7, 1980. This paper is declared a work of the U.S. Government and therefore is in the public domain.

Index categories: Boundary Layers and Convective Heat Transfer—Turbulent; Supersonic and Hypersonic Flow; Computational Methods.

*Research Scientist. Member AIAA.

†Assistant Chief, Experimental Fluid Dynamics Branch. Associate Fellow AIAA.

ber = 12×10^6-110×10^6 m^{-1}; and freestream Mach number = 2.2. The useful test time varied from 5 to 60 min depending on the total pressure.

Test Section

The test configuration shown in Fig. 1 consisted of the constant-diameter tube and a shock-generator (centerbody) which was a 15 deg half-angle cone with 6.10 cm base diameter mounted at a 15 deg angle of attack inside the tube. The shock generator could move along the centerline of the tube so the entire pressure gradient region of interest could be passed over selected measuring stations along the tube. The present measurements were obtained in a region 280-300 cm downstream from the nozzle throat. This is sufficiently downstream to establish a fully developed equilibrium turbulent boundary layer along the tube wall. The interaction of the three-dimensional shock wave produced by the shock generator with this boundary layer is the flowfield studied in this paper.

Instrumentation ports, into which interchangeable plugs could be inserted, were located at 25.4-cm intervals along the tube. These instrumentation plugs, 3.81 cm in diameter, were specially contoured to fit flush with the inner cylindrical surface of the tube. These plugs were instrumented with buried skin-friction gages, static pressure taps, and thermocouples, or a survey mechanism built to accommodate various survey probes. Additional static pressure taps were also located on a line along the tube at intervals of 5.08 cm and in the circumferential direction to verify flow symmetry upstream of the interaction. During a test run, the shock-generator was moved axially over the measurement locations. The shock-generator could be rotated between runs so data could be obtained along any given circumferential position.

The flowfield survey data were taken at sufficiently close axial stations and vertical distance away from the surface to fully document the interaction region. Data were collected at five circumferential locations; $\phi = 0$, 45, 90, 135, and 180 deg. Additional details are contained in Ref. 3.

Surface Measurements

The skin friction was measured using the buried wire technique described in Refs. 3-6. In this experiment two gage designs were used. One, similar to the buried wire gage described in Ref. 5 was used on the windward and leeward rays; the other, a bi-directional gage described in Ref. 6, was used at all five circumferential locations. The gages were calibrated in the manner described in Ref. 4. Surface angles measured from surface oil flow patterns were used to compute the skin friction in the x direction. Data from the two types of gages agreed reasonably well when compared on the most windward and leeward streamlines.

The turbulent fluctuations in both the surface pressure and skin friction were evident in the raw data obtained from these gages. Only average values of skin friction will be presented here. The experimental uncertainty in the surface pressure was estimated to be $\pm 5\%$. The skin friction accuracy was estimated to be $\pm 15\%$ in the region upstream or downstream of separation or streamwise recirculation. There are larger measurement errors in the vicinity of separation.[7]

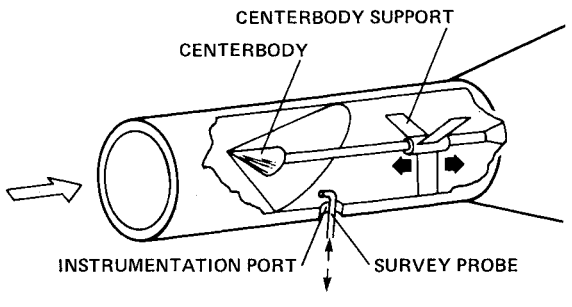

Fig. 1 Experimental test setup.

Mean-Flow Surveys

Each set of surveys along a particular circumferential data line was taken during a single test run by pre-positioning the shock generator at a given axial location and traversing the boundary layer. Along the windward ($\phi = 0$ deg) and leeward ($\phi = 180$ deg) data planes, velocity, density, and pressure profiles were obtained from pitot and static pressure surveys. Total temperature was assumed constant and equal to the freestream total temperature. Previous measurements[8] indicated that total temperature varied less than 0.5% through the boundary layer. Pitot pressures were measured on the windward and leeward data planes by a conventional pitot probe. Pitot pressure on the other data planes ($\phi = 45$, 90, and 135 deg) were obtained using a cobra probe. This probe consisted of three tubes, side by side, with the two outer tubes cut at 45 deg to the main flow. The calibration procedure is similar to that discussed in Ref. 9. Static pressure data were only obtained on the windward and leeward data planes.

To obtain the flowfield yaw angle in the various data planes, two different probes were used. One was the cobra probe just described; the other used dual hot films as the sensing element. The use of the dual hot-film gage to measure yaw angles is discussed in Ref. 10. Both probes were calibrated, then positioned at $\alpha = 0$ deg in the flowfield interaction regions and the flowfield angles obtained using the previous calibrations. The angles obtained from both probes were in excellent agreement. Further details concerning the probes employed in this investigation are contained in Ref. 3.

The experimental uncertainties in the mean-flow data in the windward and leeward planes are $\pm 10\%$ for the static pressure, $\pm 6\%$ for the static temperature, $\pm 12\%$ for density, and $\pm 3\%$ for the velocity. The uncertainties for the mean-flow data in the other planes are $\pm 3\%$ for the pitot pressure and ± 2 deg for the yaw angle. The uncertainty in y is ± 0.01 cm.

Fluctuating Measurements

Both single hot-wire and dual-wedge hot-film probes were used to obtain the three fluctuating velocity components and turbulent shear stress in the windward and leeward planes. Fluctuating measurements were made at the same locations and test conditions as the mean-flow surveys.

A single hot wire supported with an epoxy film was used to measure mass-flow fluctuations. A dual-wedge film probe was used to obtain the vertical and transverse velocity fluctuations and turbulent shear stress, as well as the flow angles in the flowfield. These probes were operated with constant temperature anemometers. A complete discussion of the calibration and data reduction techniques used for the fluctuating measurements is found in Refs. 11-13.

The experimental uncertainties in the fluctuating flowfield quantities due to the various assumptions employed and calibration errors are $\pm 15\%$.

Numerical Simulation

Governing Equations

The differential equations used to describe the mean flow for this study are the time-dependent, mass-averaged Navier-Stokes equations for a compressible fluid. Turbulent transport is included through an eddy viscosity hypothesis; that is, the Reynolds stresses and corresponding heat flux terms are assumed to be related to the mean-flow velocity and temperature gradients through an eddy transport coefficient that is simply added to the corresponding molecular transport coefficient. Zero bulk viscosity is assumed. The perfect gas equation of state is used to relate the pressure and temperature. The specific heats are assumed constant. Detailed expressions of these equations in cylindrical coordinates are presented in Ref. 3.

Turbulence Model

The turbulence effects are described using an equilibrium algebraic eddy viscosity model. The expressions for the total viscosity μ_T and the total thermal conductivity K_T are

$$\mu_T = \mu + \mu_t \quad K_T = c_p\left(\frac{\mu}{Pr} + \frac{\mu_t}{Pr_t}\right)$$

where μ is the molecular viscosity, μ_t the turbulent eddy viscosity, c_p the constant pressure specific heat, and Pr and Pr_t the molecular and turbulent Prandtl numbers, respectively. In the present investigation μ is obtained from the Sutherland viscosity relation and Pr and Pr_t are taken as 0.72 and 0.9, respectively.

The turbulent eddy viscosity used in this study is the familiar two-layer mixing-length model frequently used for calculations of two-dimensional flows.[14,15] Thus, the eddy viscosity is expressed in terms of an inner and outer eddy viscosity function as

$$\mu_t = \mu_{t_{\text{inner}}} = \rho \ell^2 \left|\frac{\partial u}{\partial y} + \frac{\partial v}{\partial x}\right| \quad \text{if } y < y_c$$

$$= \mu_{t_{\text{outer}}} = \frac{0.0168 \rho u_e \delta_i^*}{[1 + 5.5(y/\delta)^6]} \quad \text{if } y > y_c$$

where ρ is the local density, u and v velocities in the streamwise x and inward radial y directions, respectively. y_c is the first point at which $\mu_{t_{\text{inner}}}$ exceeds $\mu_{t_{\text{outer}}}$. The function ℓ is the Prandtl mixing length modified by the van Driest damping factor. For the present study no corrections for pressure gradient were applied to this mixing length.[16-18] The edge velocity u_e is set to the maximum value of u for $y < y_{\max}$; $y_{\max}$ being chosen slightly outside of the boundary layer. The boundary layer thickness δ appearing in the denominator of $\mu_{t_{\text{outer}}}$ is a constant times the compressible displacement thickness δ^*. The value of δ/δ^* used for this calculation, 3.5, was obtained from a solution of the boundary-layer equations for the upstream conditions of this flow. The solutions are not sensitive to this choice of δ since it is only used as a damping factor in μ_t. δ_i^* is the kinematic displacement thickness. Expressions for δ^* and δ_i^* are given in Ref. 3. It is felt that this turbulence model which probably contains the dominant terms and desired characteristics, would serve well as a reasonable model for this first attempt at computing this flow and as a basis for future comparison.

Computational Domain

The computational domain selected for this three-dimensional experiment consists of a cylindrical annulus with a plane of symmetry through the windward ($\phi = 0$ deg) and leeward ($\phi = 180$ deg) rays. This annular volume encompasses the fluid between two concentric cylinders 23-cm long whose radii differ by 6 cm. An exponentially stretched fine mesh is used near the wall (represented by the larger diameter cylinder) for resolving that part of the flow where viscous effects are important; the outer flow (away from the wall), which is predominantly inviscid, is described using a uniform coarse mesh. A uniform mesh is also used in the flow direction (along the axis of the cylinders). The first point in this direction is taken at 5 cm downstream from the cone tip. Uniform angles are selected for the mesh points in the circumferential or azimuthal direction.

In the azimuthal direction the mesh points are at 10-deg intervals with 20 mesh points covering the region from -5 to 185 deg. In the x direction 47 mesh points are uniformly spaced at 0.5 cm intervals. (This problem has also been solved with a 1.0 cm mesh spacing in the x direction. This coarse mesh solution showed only minor differences from the fine mesh solution reported here.) In this study 20 points were selected normal to the wall (16 of these are in the stretched fine mesh region). The first point adjacent to the wall is taken within the viscous sublayer ($y^+_{\min} \equiv y\sqrt{\tau_w \rho_w}/\mu_w \leq 1.5$). The cell closest to the wall is 0.0021 cm thick. The ratio of the size of adjacent cells in the stretched mesh region is about 1.5 to 1. Transfer from the fine to the coarse mesh in the y direction occurred near but within the outer edge of the boundary layer.

Numerical Method

The numerical procedure used here is the basic second-order, predictor-corrector, finite-difference, time-splitting method of MacCormack[19] modified by the efficient explicit-implicit-characteristic algorithm of Ref. 20. The modifications apply near the surface and result from replacing the basic explicit operator that accounts for the effects of flux in the y direction with a combination of more efficient operators. (MacCormack[21] calls this numerical technique a hybrid method.)

Reference 3 contains a detailed explanation of the hybrid method as applied to this problem as well as the operator sequencing that enabled the solution to be advanced two time steps per iteration.

The results presented here were obtained by running the numerical algorithm with a CFL of 0.9. The calculations took about 23 s per two-time-step iteration on a CDC 7600 and about 3 h of total computation time.

Boundary Conditions

At the upstream boundary the total pressure, total temperature, and freestream Mach number are chosen to correspond to experimental values for the $Re/\text{m} = 12 \times 10^6$ m^{-1} case described earlier. In the inflow boundary-layer region the velocity, density, and temperature profiles are obtained by a computer solution of the boundary-layer equations with the eddy viscosity model described previously. In this solution the displacement thickness δ^* as well as the freestream conditions are matched with the experiment. Also, at the upstream boundary, the velocities normal to the flow direction are set to zero and the freestream flow properties are held constant. Slightly unrealistic inflow conditions, such as the zero normal velocity, are quickly adjusted by the computer code within a few mesh points in the stream direction.

The boundary conditions at the wall, $y = 0$, are $u = v = w = (\partial T/\partial y) = 0$, and a finite difference approximation to the normal momentum equation at the wall is used to determine the pressure.[3,22] At the downstream boundary, zero gradient conditions are applicable throughout.

Across the symmetry plane (i.e., at $\phi = 0$ and $= 180$ deg) $w = 0$; for the other variables, the gradients with respect to ϕ are set to zero.

Along the interior cylindrical boundary, where fluid can enter or leave the computational domain, special "subsonic" boundary conditions have been applied. A solution for inviscid supersonic ($M = 2.2$) flow over a 15 deg half-angle cone at a 15 deg angle of attack was obtained from a numerical program developed by Kutler[23] to provide boundary conditions along the interior boundary. To avoid overspecifying the conditions along this boundary, a time-dependent method of characteristics is used to determine the characteristic equations for information transmitted normal to this boundary.[24] The characteristic equation along which information can reach the interior cylindrical boundary from within the computational domain is used to generate the proper boundary condition at each time step.[3] Along with this equation the pressure is assumed known at the boundary and corresponds to the values determined from the Kutler program. In addition, the isentropic relation between the pressure and the speed of sound (or the temperature) is used to determine the values of T, v and ρ on the boundary. The tangential velocities, here u and w, are determined by zero-order extrapolation for cases when the flow is out of the control volume ($v > 0$) or held fixed as determined from the Kutler code when flow is into the control volume ($v < 0$).

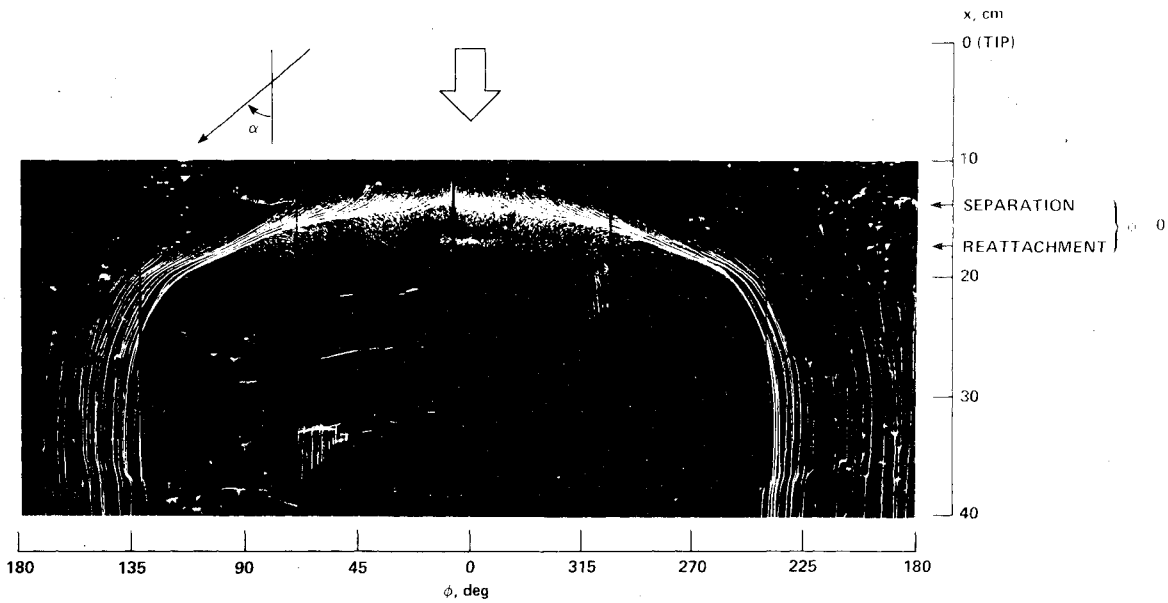

Fig. 2 Surface oil flow pattern.

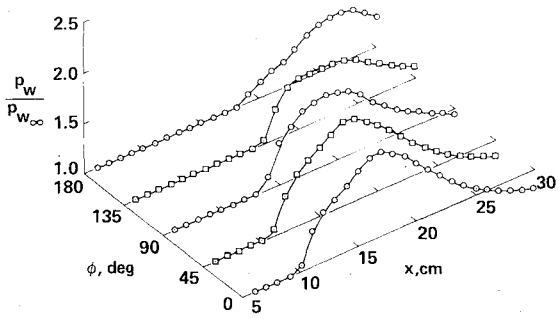

Fig. 3 Surface pressure distributions.

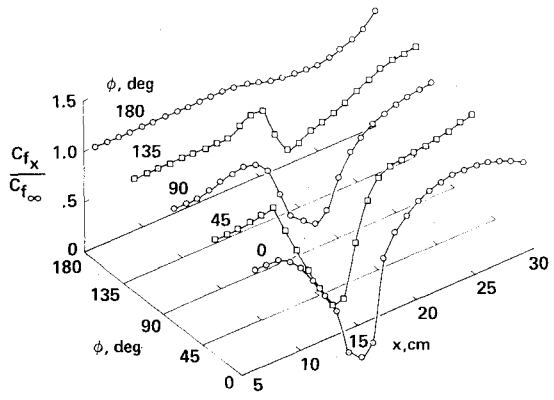

Fig. 4 Surface shear distributions.

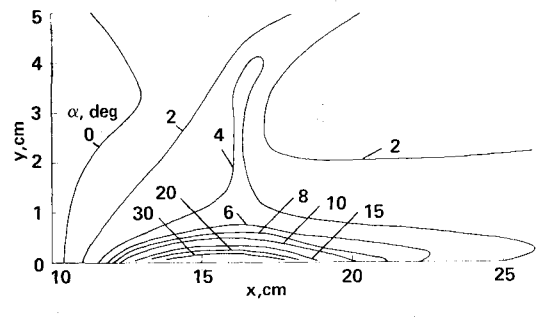

Fig. 5 Contour plot of flowfield angle, $\phi = 45$ deg.

Results and Discussion

Mean measurements of surface pressures and skin friction were made in the interaction region at several circumferential locations at three freestream Reynolds numbers, $Re/\text{m} = 12\times10^6$, 37×10^6, and 110×10^6 m^{-1}. Mean fluctuating flowfield quantities were measured at selected circumferential locations at a Re/m of 12×10^6 m^{-1}. In this paper only those results obtained at $Re/\text{m} = 12\times10^6$ m^{-1} will be presented. The surface measurements obtained at the other Reynolds numbers are discussed in Ref. 3.

Experimental Results

The three-dimensional nature of this boundary-layer flow is evident from the surface oil-flow pattern shown in Fig. 2. The trace of the shock-wave envelope on the surface is clear, along with its sweep and disappearance on the leeward side. The separation ($x = 14$ cm) and reattachment ($x = 16.8$ cm) points along the most windward ray ($\phi = 0$ deg) are shown on this oil-flow pattern. Surface flow angles were also measured directly from this flow pattern and are discussed later.

The surface pressures and average values of skin friction for five circumferential data stations are shown in Figs. 3 and 4, respectively. As one would expect from the oil flow in Fig. 2, as ϕ goes from 0 to 180 deg the initial rise in surface pressure varies with x position, starting at $x \approx 10$ cm at $\phi = 0$ deg and increasing to $x \approx 18$ cm at $\phi = 180$ deg. The maximum surface pressure $p_{w,\max}/p_{w,\infty}$ varies from 1.8 at $\phi = 0$ deg to about $p_{w,\max}/p_{w,\infty} = 1.5$ at $\phi = 180$ deg. There was no clear indication of a surface pressure plateau which is often used to imply the existence of streamwise separation. The skin-friction ratio C_{f_x}/C_{f_∞} varies dramatically at $\phi = 0$ deg; this variation diminishes to where C_{f_x} is almost constant at $\phi = 180$ deg.

In Fig. 5, a typical contour plot of the yaw angle is given for $\phi = 45$ deg. One striking feature is that the significant turning of the flow takes place in a relatively small fluid layer close to the surface—less than 15% of the boundary-layer height (~4 cm). These high turning angles are confined to the low momentum fluid which is close to the wall for turbulent boundary layers. Similar results were also observed in other three-dimensional flows by Oskam[25] and Settles.[26]

Contour plot of pressure, shear stress, and turbulent energy are presented in Figs. 6-8. A contour plot of p/p_∞ at $\phi = 0$ deg is presented in Fig. 6. Also shown in this figure (and the other contour plots to follow) are features of the flow such as the incident and "reflected" (separation and recompression) shocks, and the shape and extent of the separation bubble.

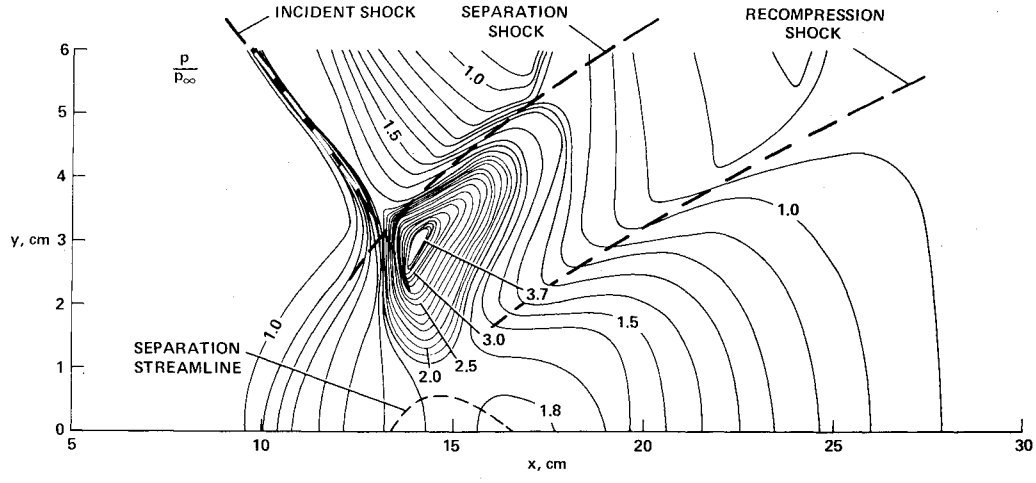

Fig. 6 Contour plot of static pressure ratio, $\phi = 0$ deg.

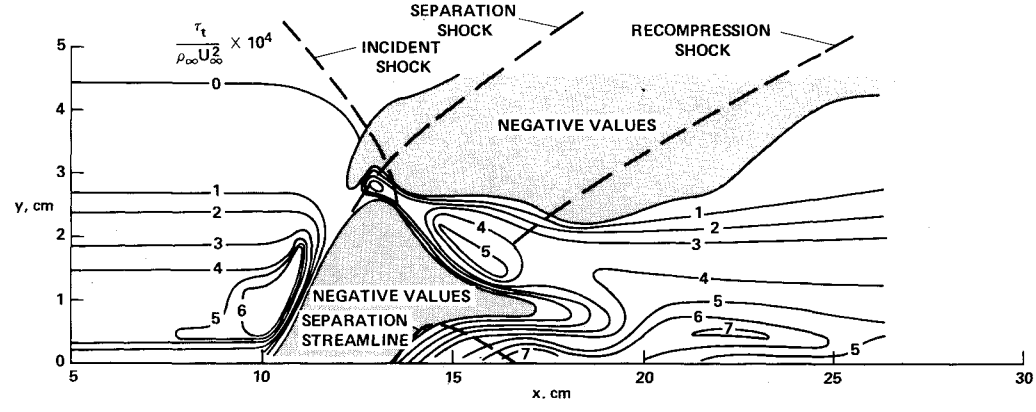

Fig. 7 Contour plot of turbulent shear stress, $\phi = 0$ deg.

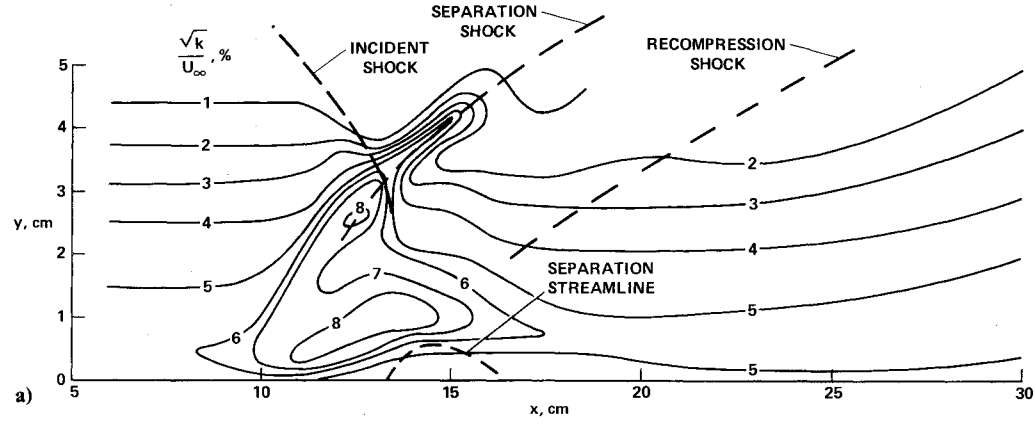

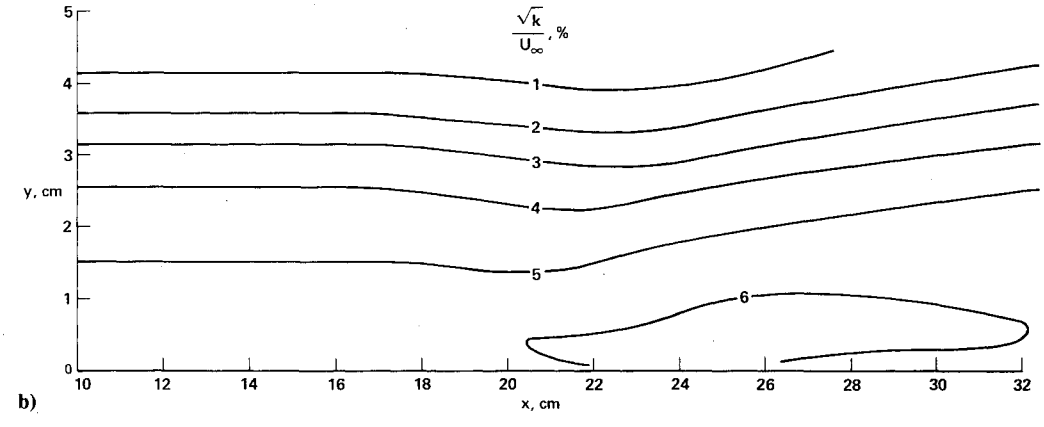

Fig. 8 Contour plot of turbulent kinetic energy: a) $\phi = 0$ deg, and b) $\phi = 180$ deg.

The flow details are vividly portrayed in this plot, and such features as the high pressure peak near the confluence of the incident and separation shocks are evident.

The contour plot of the turbulent shear stress in the flowfield at $\phi = 0$ deg is shown in Fig. 7. The shaded area represents negative turbulent shear stress. These negative values are surprising since, for the most part, du/dy is positive in the regions of negative shear stress. This implies that the eddy-viscosity concept of modeling the shear stress is not correct in the vicinity of the separation bubble. These findings, however, may result from the assumptions used in the data reduction technique rather than from the flowfield. To obtain the shear stress from a hot-wire measurement in compressible flow an assumption must be made concerning the fluctuating pressure and its correlations with velocity and temperature.[13] The assumption employed here was that the pressure vertical-velocity correlation is negligible. This assumption may not be valid in the vicinity of a shock wave, although Johnson and Rose[27] have shown its validity both upstream and downstream of a shock wave. Further tests employing both a hot wire and a laser velocimeter are required to validate the present results. However, recent laser velocimeter measurements[28] in the vicinity of a shock wave have also shown negative values of the shear stress in regions of the flow where du/dy is positive. Measured values of the shear stress at $\phi = 180$ deg showed little variation in the axial direction.

Contour plots of the turbulent kinetic energy at $\phi = 0$ and 180 deg are shown in Figs. 8a and 8b. Peak kinetic energies at $\phi = 0$ deg appear in the region of the convergence of the incident and separation shock and in the region immediately above the bubble. These peaks are about 50% higher than the maximum kinetic energy in the undisturbed flow. For several two-dimensional turbulent boundary-layer, shock-wave interaction flows, increases in kinetic energy in the interaction regime over that in the undisturbed flow of 130% at $M_\infty = 1.44$ (Ref. 24), 300% at $M_\infty = 2.25$ (Ref. 29), and 400% at $M_\infty = 3$ (Ref. 30) have been reported. The significant differences between the large kinetic energy increases observed in two-dimensional flow and the much smaller increase observed in the present three-dimensional flow investigation could be attributed to the fact that the two-dimensional flows are geometrically constrained whereas the present three-dimensional flow (or perhaps any three-dimensional flow) is not.

Large differences can be noted in the behavior of the turbulent shear stress and kinetic energy on the most windward ray ($\phi = 0$ deg). While the kinetic energy only increased 50% over the maximum upstream values, the shear stress went through large variations (sometimes negative) throughout the flowfield; far downstream it still retained some of its previous interaction region history. On the leeward data line ($\phi = 180$ deg) the turbulent kinetic energy varies slightly from the equilibrium values measured upstream.

Numerical Results

Numerical results are compared with experimental measurements for $Re/m = 12 \times 10^6$ m^{-1} in Figs. 9-13. The computed surface pressure is compared with the corresponding experimental results at various axial and azimuthal positions in Fig. 9. Overall behavior of the pressure with the position is well predicted by the numerical results as are the location and magnitude of the peak pressure along each azimuth. However, the streamwise location of the initial pressure rise at the smaller values of ϕ is not predicted. The calculations underpredict the initial pressure rise on the windward side ($\phi = 0$ deg) of the cone and overpredict it on the leeside ($\phi = 180$ deg). Thus, a footprint of the shock on the surface would show that, relative to the computed shock, the measured shock would have more downstream curvature with ϕ (i.e., the pressure rise begins further upstream for small ϕ and further downstream for large ϕ). The initial pressure rise is best predicted for $\phi = 90$ deg, but the associated axial pressure gradient is less than the measured pressure gradient.

Comparisons between calculated and measured values of skin friction for various axial and azimuthal locations are presented in Fig. 10. The overall skin-friction predictions agree quite well with the experimental measurements. Variations of the calculated results with ϕ and x are in qualitative (if not quantitative) agreement with the data. The computation predicts the location and extent of separation on the windward side ($\phi = 0$ deg) quantitatively well, but predicts a reverse flow regime slightly upstream of the measurements at $\phi = 45$ deg, and predicts reversed flow when none is measured at $\phi = 90$ deg. (This was the largest ϕ for which the calculations showed flow reversal.) The overall shape of the reversed flow region on the surface is correct (moving downstream with increasing ϕ), but the numerical results predict a larger lateral extent than the measurements show.

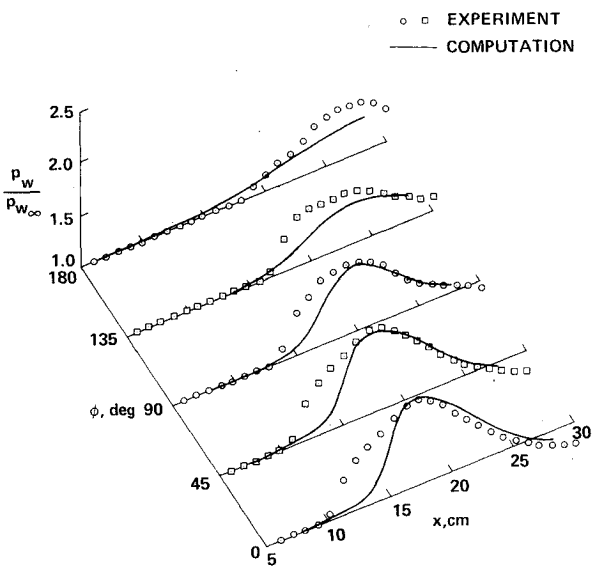

Fig. 9 Surface pressure distribution—comparison of experiment with computations.

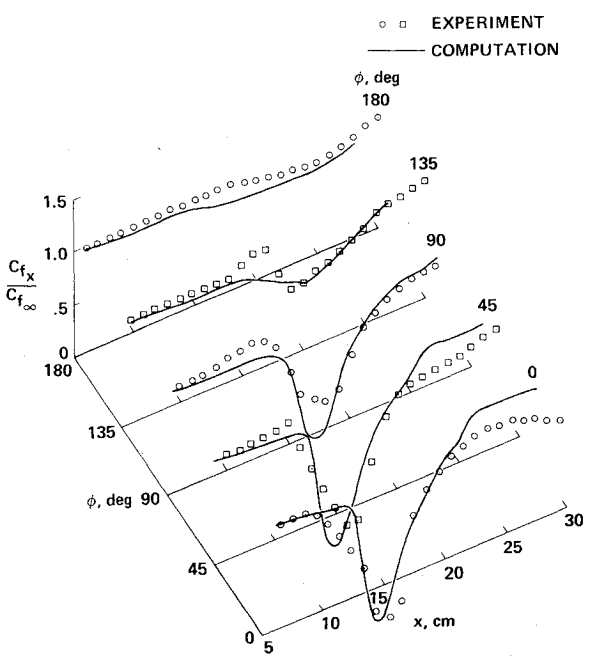

Fig. 10 Surface shear distribution—comparison of experiment with computations.

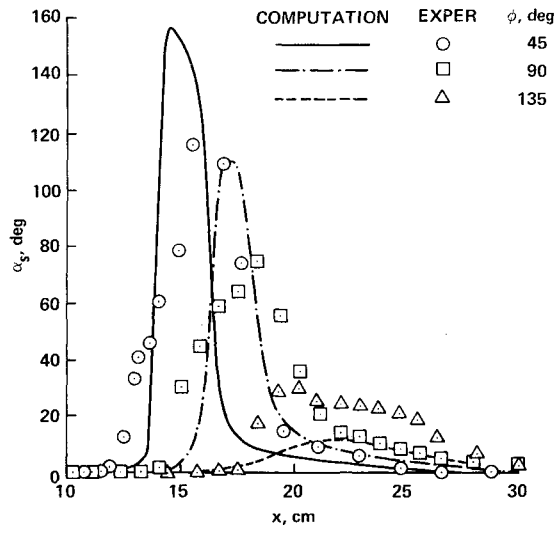

Fig. 11 Surface skin-friction line angles—comparison of experiment with computations.

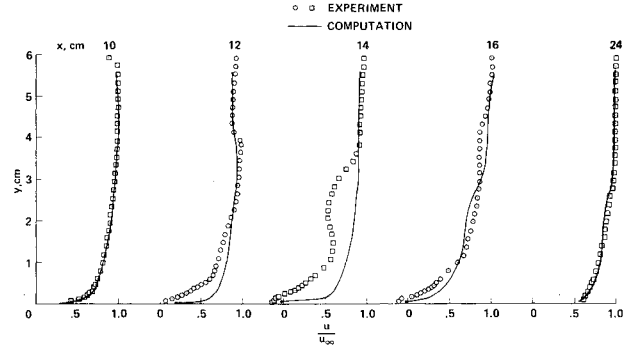

Fig. 12 Velocity profiles across the flowfield—comparison of experiment with computations, $\phi = 0$ deg.

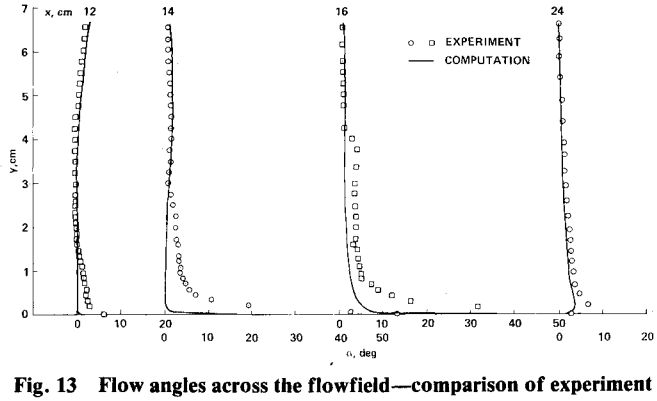

Fig. 13 Flow angles across the flowfield—comparison of experiment with computations, $\phi = 45$ deg.

On the leeside little variation in C_f occurs in the flow direction and the predictions concur.

In Fig. 11 the surface skin-friction angles are compared with calculated results for $\phi = 45$, 90, and 135 deg. This figure shows qualitative agreement between calculations and measurements and somewhat illustrates the extent to which the calculations overpredict the reversed flow region on the surface.

Calculated and measured velocity profiles at various axial positions along the windward azimuth are compared in Fig. 12. This comparison shows that upstream and downstream of the interaction the profile is predicted very well. However, in the interaction region the profiles are not predicted well. The differences between the measured and calculated profiles at $x = 12$, 14 and 16 cm are associated with the pressure differences shown along $\phi = 0$ in Fig. 9. That is, relative to the computations, the experimental flow has a significantly higher pressure near the surface for $10 < x < 15$ cm. This disparity in pressures is possibly due to the simple turbulence model used in the calculations; however, the lack of numerical resolution normal to the tunnel axis might also be a contributing factor. Both these aspects will be investigated in the future. The comparisons in Fig. 12 also illustrate that the computed reversed flow region is considerably thinner and the magnitude of the reversed velocities is less than the experimental results.

In Fig. 13, a comparison is shown between measured and calculated flowfield angles at an azimuth of 45 deg. Both the experiment and the computations show that most of the turning of the flow occurs near the surface where the flow angle differences are due to the calculated reversed flow region being thinner than the measurements indicate. Away from the surface the relatively larger measured turning angles at each x, ϕ location is a result of the greater thickness of the experimental reversed flow region. This thickness produces larger disturbances in the flowfield, resulting in increased pressure and flow turning angles. This is also the case at the $\phi = 90$ and 135 deg positions.[3]

It should be noted that some of the differences observed between the calculated and experimental results in Figs. 9 and 12 for this three-dimensional flow are similar to observations made for two-dimensional flows. That is, when the present algebraic turbulence model is used for two-dimensional shock-boundary-layer interaction flows, the calculated separation region is very shallow and the pressure plateau is absent in comparison with experimental measurements.[14,31] For these two-dimensional flows, improved results were obtained when more sophisticated turbulence models were included in the analysis.[14] These multiequation turbulence models will be included in the calculations for the present flow in the near future.

Concluding Remarks

To test the validity of existing and proposed computer codes and their associated turbulence models, an experiment was devised in which a three-dimensional shock wave impinged on an axisymmetric boundary layer resulting in a complex three-dimensional separated flow. Sufficient measurements were made of both mean and fluctuating flow quantities on the surface and in the flowfield to completely document the flow. The experimental flow itself was a fairly complicated one, wherein the three-dimensional shock wave from a sharp cone at angle of attack at $M_\infty \approx 2.2$ interacted with an axisymmetric turbulent boundary layer resulting in a large three-dimensional separated flow. The large reversed flow region along the windward plane ($\phi = 0$ deg) became progressively smaller and disappeared at about $\phi \approx 90$ deg. Most of the fluid turning in the flowfield was confined to a relatively thin layer close to the surface where the low momentum fluid resides in a turbulent boundary layer. Another interesting result was the large difference noted in the behavior of the turbulent shear stress and kinetic energy on the most windward ray ($\phi = 0$ deg). While the kinetic energy only increased 50% over the upstream values, the shear stress went through large variations (sometimes negative) throughout the flowfield and still retained some of its previous interaction region history far downstream.

The time-dependent compressible Navier-Stokes equations were solved for this flow by an efficient mixed explicit-implicit numerical method. In this solution an algebraic eddy viscosity model was used to model the turbulence. The numerical results were in reasonably good agreement with measurements considering the complexity of the flowfield. Quantitative differences between the numerical predictions

and the measurements can be attributed in large measure to the simple turbulence model used in this study. The differences in surface pressure, velocity, skin friction, and flow angle manifest themselves primarily in the strong interaction region where the flow is reversed. Similar quantitative differences between predictions and measurements have been observed for two-dimensional flows when a similar turbulence model was employed. In these two-dimensional cases markedly improved results were obtained when more versatile multiequation turbulence models were used. It is expected that similar improvements would appear in the present calculations when these more sophisticated turbulence models are incorporated. This task along with improvements in numerical resolution is presently being pursued.

Acknowledgment

The authors are grateful to R. W. MacCormack and T. J. Coakley for their valuable discussions and suggestions on the numerical techniques.

References

[1] Marvin, J. G., "Turbulence Modeling for Compressible Flows," NASA TM X-73, 188, 1977.

[2] Horstman, C. C. and Hung, C. M., "Computation of Three-Dimensional Turbulent Separated Flows at Supersonic Speeds," AIAA Paper 79-0002, New Orleans, La., Jan. 1979.

[3] Kussoy, M. I., Viegas, J. R., and Horstman, C. C., "An Experimental and Numerical Investigation of a 3-D Shock Separated Turbulent Boundary Layer," AIAA Paper 80-0002, Pasadena, Calif., Jan. 1980.

[4] Acharya, M., Kussoy, M. I., and Horstman, C. C., "Reynolds Number and Pressure Gradient Effects on Compressible Turbulent Boundary Layers," AIAA Paper 78-199, Huntsville, Ala., Jan. 1978.

[5] Rubesin, M. W., Okuno, A. F., Mateer, G. G., and Brosh, A., "A Hot Wire Surface Gage for Skin Friction and Separation Detection Measurements," NASA TM X-62,465, 1975.

[6] Higuchi, H. and Peake, D. J., "Bi-Directional, Buried-Wire Skin Friction Gage," NASA TM-78531, 1978.

[7] Owen, F. K. and Johnson, D. A., "Separated Skin Friction Measurement—Source of Error, and Assessment, and Elimination," AIAA Paper 80-1409, Snowmass, Colo., July 1980.

[8] Kussoy, M. I., Horstman, C. C., and Acharya, M., "An Experimental Documentation of Pressure Gradient and Reynolds Number Effects on Compressible Turbulent Boundary Layers," NASA TM-78488, 1978.

[9] Dudzinski, T. J. and Krause, L. N., "Flow Direction Measurements with Fixed-Position Probes," NASA TM X-1904, 1969.

[10] Helms, V. T., III, "Measurements of Flow Angle and Mass Flow Rate in an Unknown Flow Field Using Hot Film and Hot Wire Probes," AIAA Paper 78-794, San Diego, Calif., 1978.

[11] Acharya, M., Horstman, C. C., and Kussoy, M. I., "Reynolds Number Effects on the Turbulence Field in Compressible Boundary Layers," *AIAA Journal*, Vol. 17, April 1979, pp. 380-386.

[12] Acharya, M., "Measurement of Turbulent Fluctuations in High-Speed Flows Using Hot Wires and Hot Films," *Review of Scientific Instruments*, Vol. 50, Aug. 1979, pp. 952-957.

[13] Horstman, C. C. and Rose, W. C., "Hot-Wire Anemometry in Transonic Flow," *AIAA Journal*, Vol. 15, March 1977, pp. 395-401.

[14] Viegas, J. R. and Horstman, C. C., "Comparison of Multiequation Turbulence Models for Several Shock Boundary-Layer Interaction Flows," *AIAA Journal*, Vol. 17, Aug. 1979, pp. 811-820.

[15] Horstman, C. C., Kussoy, M. I., Coakley, T. J., Rubesin, M. R., and Marvin, J. G., "Shock-Wave-Induced Turbulent Boundary-Layer Separation at Hypersonic Speeds," AIAA Paper 75-4, Pasadena, Calif., Jan. 1975.

[16] Horstman, C. C., Settles, G. S., Vas, I. E., Bogdonoff, S. M., and Hung, C. M., "Reynolds Number Effects on Shock-Wave Turbulent Boundary-Layer Interactions," *AIAA Journal*, Vol. 15, Aug. 1977, pp. 1152-1158.

[17] Reynolds, W. C., "Computation of Turbulent Flows," *Annual Review of Fluid Mechanics*, Vol. 8, 1976, pp. 183-208.

[18] Rubesin, M. W., Crisalli, A. J., Horstman, C. C., Acharya, M., and Lanfranco, M. J., "A Critique of Some Recent Second Order Closure Models for Compressible Boundary Layers," AIAA Paper 77-128, Los Angeles, Calif., Jan. 1977.

[19] MacCormack, R. W., "Numerical Solution of the Interaction of a Shock Wave with a Laminar Boundary Layer," *Lecture Notes in Physics*, Vol. 8, Springer-Verlag, New York, 1971, pp. 151-163.

[20] MacCormack, R. W., "An Efficient Numerical Method for Solving the Time-Dependent Compressible Navier-Stokes Equations at High Reynolds Number," *Computing in Applied Mechanics*, AMD Vol. 18, The American Society of Mechanical Engineers, 1976.

[21] MacCormack, R. W., "Status and Future Prospects of Using Numerical Methods to Study Complex Flows at High Reynolds Numbers," AGARD-LSP-94, Feb. 1978.

[22] MacCormack, R. W. and Baldwin, B. S., "A Numerical Method for Solving the Navier-Stokes Equations with Application to Shock-Boundary-Layer Interactions," AIAA Paper 75-1, Jan. 1975.

[23] Kutler, P., Reinhardt, W. A., and Warming, R. F., "Multishocked, Three-Dimensional Supersonic Flowfields with Real Gas Effects," *AIAA Journal*, Vol. 11, May 1973, pp. 657-663.

[24] Mateer, G. G., Brosh, A., and Viegas, J. R., "A Normal Shock-Wave Turbulent Boundary-Layer Interaction at Transonic Speeds," AIAA Paper 76-161, Wash., D.C., 1976.

[25] Oskam, B., Bogdonoff, S. M., and Vas, I. E., "Oblique Shock Wave/Turbulent Boundary Layer Interactions in Three Dimensions at Mach 3," AFFDL-TR-76-48, Air Force Flight Dynamics Laboratory, June 1976.

[26] Settles, G. S. and Perkins, J. J., "Investigation of Three-Dimensional Shock/Boundary Layer Interactions at Swept Compression Corners," AIAA Paper 69-1498, Williamsburg, Va., July 1979.

[27] Johnson, D. A. and Rose, W. C., "Laser Velocimeter and Hot-Wire Anemometer Comparison in a Supersonic Boundary Layer," *AIAA Journal*, Vol. 13, April 1975, pp. 512-515.

[28] Marvin, J. G., Levy, L. L., Jr., and Seegmiller, H. L., "On Turbulence Modeling for Unsteady Transonic Flows," *AIAA Journal*, Vol. 18, May 1980, pp. 489-496.

[29] Ardonceau, P., Lee, D. H., de Roquefort, T. A., and Goethals, R., "Turbulence Behavior in a Shock Wave/Boundary Layer Interaction," AGARD Conference Preprint 271, *Turbulent Boundary Layers—Experiments, Theory, and Modelling*, 1979.

[30] Bachalo, W. D., Modarress, D., and Johnson, D. A., "Experiments on Transonic and Supersonic Turbulent Boundary Layer Separation," AIAA Paper 77-47, Los Angeles, Calif., Jan. 1977.

[31] Coakley, T. J., Viegas, J. R., and Horstman, C. C., "Evaluation of Turbulence Models for Three Types of Shock Separated Boundary Layers," AIAA Paper 77-692, Albuquerque, N. Mex., 1977.